From pre- to young planetary nebulae: radio continuum variability

L. Cerrigone,[1]⋆ C. Trigilio,[2] G. Umana,[2] C. S. Buemi[2] and P. Leto[2]

[1]*Max-Planck-Institut für Radioastronomie, Auf dem Hügel 69, 53121 Bonn, Germany*
[2]*INAF-Osservatorio Astrofisico di Catania, via S. Sofia 78, 95123 Catania, Italy*

ABSTRACT

Searching for variability, we have observed a sample of hot post-asymptotic giant branch stars and young planetary nebula candidates with the Very Large Array at 4.8, 8.4 and 22.4 GHz. The sources had been previously detected in the radio continuum, which is a proof that the central stars have started ionizing their circumstellar envelopes, and an increase in radio flux with time can be expected as a result of the progression of the ionization front. Such a behaviour has been found in IRAS 18062+2410, whose radio modelling has allowed us to determine that its ionized mass has increased from 10^{-4} to $3.3 \times 10^{-4}\,M_\odot$ in 8 yr and its envelope has become optically thin at lower frequencies.

Different temporal behaviours have been found for three other sources. IRAS 17423−1755 has shown a possibly periodic pattern and an inversion of its radio spectral index, as expected from a varying stellar wind. We estimate that the radio flux arises from a very compact region around the central star ($\sim 10^{15}$ cm) with an electron density of $2 \times 10^6\,cm^{-3}$. IRAS 22568+6141 and IRAS 17516−2525 have decreased their radio flux densities by about 10 per cent per year over 4 yr.

While a linear increase in the flux density with time points to the progression of the ionization front in the envelope, decreases as well as quasi-periodic patterns may indicate the presence of unstable stellar winds/jets or thick dusty envelopes absorbing ionizing photons.

Key words: stars: AGB and post-AGB – circumstellar matter – radio continuum: stars.

1 INTRODUCTION

The evolution of planetary nebulae (PNe) remains a challenging topic in astrophysics. PNe have been observed over a wide wavelength range, from X-ray to radio frequencies. Their complex morphologies and the shaping mechanisms that produce them are still a matter of debate. Companion stars, jets from central stars, magnetic fields, dust tori and interacting winds are some of the possible shaping agents suggested as being responsible for various PN morphologies, and an overlap of their actions cannot be ruled out (Kwok 2000b).

In general, the current theory of PN evolution is based on the interacting stellar wind (ISW) model (Kwok, Purton & Fitzgerald 1978) and its generalized version (Kahn & West 1985). The ISW model encompasses a high-velocity stellar wind driven by the hot central star that runs into the lower velocity expanding circumstellar envelope (CSE) remaining from the earlier asymptotic giant branch (AGB) phase. However, this model does not account for the shaping, because it assumes that an asymmetric distribution of matter is already present when the wind interaction occurs. Other models

take into account the possible role of jets and have been successfully applied to some nebulae (Sahai & Trauger 1998). It has been suggested that the interaction with a companion object, even a massive planet, may provide the necessary asymmetry (Soker 2006). Also, large-scale magnetic fields, influencing or determining the shapes, might be sustained by a dynamo process (Blackman et al. 2001).

The birth of a PN is defined by the formation of an ionization front, which is itself a shaping agent and could heavily influence the morphology established in earlier evolutionary phases. In this context, important information can be provided by observations of very young PNe and pre-PNe with hot central stars, where the physical processes associated with PN formation are still occurring. The term 'young PNe' is often used in the literature for nebulae like NGC 7027, which hosts a central star with $T_{eff} \sim 2 \times 10^5$ K. When we use this term in this work, we actually indicate much cooler objects, which show in their optical spectra only recombination and low-excitation emission lines (see e.g. the spectra of some of our targets in Suárez et al. 2006).

To investigate the properties of these rare objects in transition from the post-AGB to the PN, we have selected a sample of pre-PN and young-PN candidates and searched for radio emission from ionized shells (Umana et al. 2004; Cerrigone et al. 2008). The targets were selected from stars classified in the literature as hot

⋆E-mail: lcerrigone@mpifr.de

post-AGB candidates, showing strong far-infrared (far-IR) excess and B spectral type features. The detection of radio continuum emission is a proof of the presence of free electrons and therefore of ionization. Multifrequency observations allow for a characterization of the origin of the emission (i.e. different spectral indices point to different physical conditions).

The progression of ionization in the envelope around the star can be observed as an increase in the ionized mass with time, which implies an increasing radio flux density. A few objects have been observed frequently enough to allow for such an investigation. For example, CRL 618 has been observed for many years at centimetre and millimetre wavelengths and appears to show time-intervals of increasing and decreasing flux density (Sánchez-Contreras et al. 2004). SAO 244567 is another transition object that shows a decrease in radio flux density over a few years (Umana et al. 2008) instead of an increase, as expected on the basis of its last 40 yr of evolution (Bobrowsky et al. 1999). Several works monitoring this class of objects in the Hα indicate that the onset of ionization may be accompanied by variability whose origin is not clear (Arkhipova et al. 2001), while variability due to stellar pulsations has been found in post-AGB stars of F and G spectral types (Hrivnak et al. 2010).

For a better understanding of this particular phase, we have observed again all of the targets detected in our previous works looking for radio variability. Six new targets following the same selection criteria of the original sample were also observed in this work, after we detected radio emission from them in a previous observing run.

2 OBSERVATIONS

We observed our targets with the Very Large Array (VLA) operated by the National Radio Astronomy Observatory (NRAO) at 4.8, 8.4 and 22.4 GHz. The observations were scheduled dynamically and only five sources were observed at the highest frequency, because of weather conditions and limited time available in the dynamic queue in our RA range.

The runs at the lower frequencies (4.8 and 8.4) were performed in 2009 June in the CnB and C configurations, and during reconfiguration time. Each target was observed for about 10 min, preceded and followed by 2 min on a nearby phase calibrator. The absolute flux density scale was defined by observing 3C48 or 3C286, depending on which of the two calibrators was observable when the run was carried out. The same flux calibrators were used in the 22.4-GHz runs carried out in 2009 September (DnC array) and December (D array). At the highest frequency, fast switching between the target and the phase calibrator was implemented to allow for a proper phase calibration. The on-source time was also about 10 min.

The data were reduced with the Astronomical Image Processing System (AIPS), according to the recommended reduction process: the data sets were FILLMed into AIPS with an average opacity correction and nominal sensitivities (doweight = 1), edited to flag interference or any other bad points and CALIBrated along with point weights (docalib = 2). Observations performed in different days were reduced separately and antenna positions were corrected with the task VLANT. Since both VLA and EVLA antennas were included in the array, a baseline-dependent calibration was performed for each calibrator (task BLCAL) and the solutions were then applied in the usual calibration process, to avoid excessive closure errors. Models of both 3C48 and 3C286 were used at all frequencies to properly set the absolute flux density scale. Maps were obtained using the task IMAGR with natural weights and CLEANed by performing a few hundred iterations of the CLEAN algorithm.

The flux density for each source was estimated by fitting a Gaussian to the unresolved source (task JMFIT) and the rms noise was calculated in an area much larger than the synthesized beam (>100 beam), without evident sources in it (task IMEAN). One source (IRAS 22568+6141) was resolved in two close peaks. In this case, the data were first tapered to obtain one unresolved source and then a Gaussian was fitted, to estimate the total flux density. To better analyse the single peaks, at 4.8 and 22.4 GHz, the Gaussian fitting was performed on maps obtained with uniform weighting (robust = −5) to improve the angular resolution and distinguish the peaks. In spite of the uniform weighting, at 22.4 GHz, the peaks overlap; in this case, the task JMFIT has been used to simultaneously fit two Gaussians. The Gaussians thus obtained are centred on the same coordinates as those at the other frequencies within about 0.2 arcsec, which confirms that the task correctly identifies the components.

3 RESULTS

We summarize in Table 1 the flux densities obtained and their relative variation per year. The errors reported in the table contain a 3 per cent absolute calibration error, $\sigma = \sqrt{\mathrm{rms}^2 + (0.03F_\nu)^2}$. We have compared these new results with the values reported in Umana et al. (2004) and Cerrigone et al. (2008), looking for variability. About half of the targets exhibit stable radio fluxes and only one is clearly variable: IRAS 18062+2410. As 'clearly variable', we mean that at both 4.8 and 8.4 GHz we observe a relative variation larger than three times its error. Variability in at least one band is observed in six targets, if this criterion is loosened to twice the error. Since the variations are only in one band, it is unclear whether this is due to observational errors or an intrinsic change in the emission.

For IRAS 22568+6141, which is resolved into two blobs of emission, we list in Table 1 the flux densities of its northern and southern lobe as well as the emission from the whole nebula. As explained in the previous section, the flux density of the whole nebula was obtained by fitting a Gaussian on a tapered map, where the source is not resolved. The sum of the flux densities of the two blobs does not account for the emission of the entire nebula. An inspection of the residual maps (the maps after subtraction of the fitting Gaussians) indicates that about 4.3 mJy at 4.8 GHz and 0.5 mJy at 8.4 GHz remain unmatched. This means that – besides the two peaks – weak extended emission is present and is recovered by tapering.

We performed for the first time multifrequency observations of IRAS 01005+7910, 17516−2525, 21546+4721, 22023+5249, 22495+5134 and 22568+6141 (Fig. 1).

We fitted the data points to derive the spectral indices, which turned out to match very well with what expected for optically thin shells ($\alpha \sim -0.1$), as can be seen in Table 2. Since the emission is optically thin, we can also derive the emission measure for each of these sources as

$$\langle EM \rangle = \frac{\int_\Omega EM d\Omega}{\Omega} = \frac{5.3 \times 10^5 F_{8.4\,\mathrm{GHz}}}{\theta^2},$$

where $F_{8.4\,\mathrm{GHz}}$ is the flux density at 8.4 GHz in mJy and θ is the angular radius in arcsec (Terzian & Dickey 1973). The only target that is resolved at our angular resolution is IRAS 22568+6141 (Section 7), whose northern and southern blobs of emission are listed separately in Table 2. Gaussian fitting of the two peaks allows us to determine their positions as RA = 22^{h}58^{m}51^s.44 Dec. = 61°57′45″.2 (north

Table 1. Radio flux densities obtained at the VLA and their relative variations per year. Targets that do not show variations are listed first, then targets that show variations at least in one band. For IRAS 22568+6141, the flux densities of its northern and southern lobes are also listed.

IRAS ID	$F_{4.8\,\mathrm{GHz}}$ (mJy)	$\Delta F_{4.8\,\mathrm{GHz}}$ (per cent per year)	$F_{8.4\,\mathrm{GHz}}$ (mJy)	$\Delta F_{8.4\,\mathrm{GHz}}$ (per cent per year)	$F_{22.4\,\mathrm{GHz}}$ (mJy)
01005+7910	0.29 ± 0.05	–	0.17 ± 0.04	−4.3 ± 4.9	–
17381−1616	1.64 ± 0.08	0.3 ± 1.2	1.62 ± 0.07	2.3 ± 1.4	–
19336−0400	11.1 ± 0.3	1.1 ± 1.0	9.5 ± 0.3	−0.3 ± 1.0	–
19590−1249	3.3 ± 0.1	1.1 ± 1.3	3.1 ± 0.1	1.6 ± 0.9	–
20462+3416	0.62 ± 0.05	0.7 ± 2.0	0.43 ± 0.04	0.4 ± 2.6	–
21546+4721	1.56 ± 0.06	–	1.56 ± 0.06	0.6 ± 1.4	1.32 ± 0.07
22023+5249	2.60 ± 0.09	–	2.28 ± 0.08	2.3 ± 1.2	2.1 ± 0.1
22495+5134	9.6 ± 0.3	–	8.6 ± 0.3	0.8 ± 1.2	8.1 ± 0.3
06556+1623	0.45 ± 0.05	−4.1 ± 1.5	0.48 ± 0.04	−2.1 ± 1.5	0.11[a]
17423−1755	0.63 ± 0.06	–	0.50 ± 0.05	15.4 ± 4.8	–
17460−3114	1.4 ± 0.1	−1.7 ± 1.4	1.08 ± 0.07	−2.7 ± 1.3	–
17516−2525	0.4 ± 0.1[b]	–	0.32 ± 0.06	−11.6 ± 2.8	–
18062+2410	1.72 ± 0.08	4.9 ± 1.5	2.67 ± 0.09	13.8 ± 2.2	–
18442−1144	21.7 ± 0.7	3.7 ± 1.2	20.7 ± 0.6	1.3 ± 1.0	–
22568+6141	23.8 ± 0.7	–	21.7 ± 0.7	−8.1 ± 0.7	16.0 ± 0.5
22568+6141 N	10.0 ± 0.3	–	11.2 ± 0.3	–	8.5 ± 0.2
22568+6141 S	9.8 ± 0.3	–	9.3 ± 0.3	–	7.3 ± 0.3

[a] The source was not detected and the rms of the map is listed.
[b] Marginal detection.

peak) and RA = $22^\mathrm{h}58^\mathrm{m}51\overset{\mathrm{s}}{.}68$ Dec. = $61°57'42\overset{''}{.}8$ (south peak). The peaks are about 3 arcsec apart, with PA ∼ 146°.

To calculate their emission measures, we need to estimate the angular sizes of our sources. In Table 2, we list the major and minor axes of the convolution beam. For those sources that have been resolved with high angular resolution observations in Cerrigone et al. (2008) (IRAS 18442−1144, 19336−0400, 19590−1249 and 22023+5249), the geometric mean of the axes is an approximate estimation of their diameters; therefore, we take into account this value in our calculations.

4 IRAS 17423−1755

IRAS 17423−1755 (Hen3-1475) is a well-known point-symmetric pre-PN at a distance of about 5.8 kpc. It shows OH maser emission, lines from ionized elements and recombination lines due to shocks propagating in its CSE (Riera et al. 2003). Sánchez Contreras & Sahai (2001) find that two wind components are present in the vicinity of the star (∼0.7 arcsec): a fast and an ultrafast wind (150–1200 and 2300 km s^{-1}, respectively), both with kinematical ages of tens of years. Decreasing velocities from 1000 to 150 km s^{-1} are found in the knots in its bipolar outflow, traced by optical and near-IR imaging over 17 arcsec (Riera et al. 2003). Millimetre and centimetre observations trace much smaller structures, likely associated to a circumstellar disc (millimetre observations) and a compact ionized region (centimetre observations) (Huggins et al. 2004).

Several models have been applied to this source to account for its kinematical and morphological properties. A possible explanation is that its peculiarities are the result of an ejection variability of the central source (Riera et al. 2003). Velázquez, Riera & Raga (2004) have modelled this nebula with a precessing jet of periodically variable ejection velocity superimposed to a linear increase, which propagates into an interstellar medium previously perturbed by an AGB wind. The velocity variability in their model has a period of 120 yr and a half-amplitude of 150 km s^{-1}. The jet has therefore an

ejection velocity of the form $v_\mathrm{jet} = v_0 + v_1 \sin[2\pi(t-t_0)/\tau] + at$, with $v_0 = 400\,\mathrm{km\,s^{-1}}$, $v_1 = 150\,\mathrm{km\,s^{-1}}$, $t_0 = -640\,\mathrm{yr}$, $\tau = 120\,\mathrm{yr}$ and $a = 1\,\mathrm{km\,s^{-1}\,yr^{-1}}$.

Lee & Sahai (2003) present a general model to shape pre-PNe with collimated fast winds interacting with a spherical AGB wind and they compare their results with observations of CRL 618. They introduce periodic variations of the density and velocity of the fast wind in such a way that the mass-loss rate ($\dot{M} = 4\pi r^2 \rho v$) is kept constant: the density varies as $\rho = \frac{\rho_\mathrm{f}}{1 + A\sin\frac{2\pi t}{\tau}}$ and the velocity as $v = v_\mathrm{f}(1 + A\sin\frac{2\pi t}{\tau})$. In particular, to compare their model to CRL 618, they consider a period of 22 yr and a velocity half-amplitude of 150 km s^{-1}.

Radio continuum data since 1991 are available in the VLA archive. We retrieved the data, reduced them following the same recipe as for the rest of our data and found a flux density of 0.36 ± 0.04 mJy in 1991 and 0.56 ± 0.04 mJy in 1993, both at 8.4 GHz. As shown in Fig. 2, the combination of our 2001 and 2009 observations with the archive data clearly shows variability of the radio flux density. Unfortunately, our temporal sampling is too coarse to conclusively assess whether the variability is regular or not. Nevertheless, we show that the data are well fitted by periodic functional forms similar to those introduced by Velázquez et al. (2004) and Lee & Sahai (2003):

$$S_\nu = A_0 \sin\frac{2\pi}{A_1}t + A_2 \qquad \text{(dotted line)}$$

$$S_\nu = \frac{A_0}{1 + A_1 \sin\frac{2\pi}{A_2}t} \qquad \text{(dashed line)}$$

We are fitting four points with functions having three degrees of freedom; therefore, the procedure should not be overinterpreted. Both fits give periods of around 19 yr (18.6 and 18.7 yr, for the dashed and dotted curves, respectively), comparable to the periodicity in the model of CRL 618 by Lee & Sahai (2003), but different from the period introduced in the model of IRAS 17423−1755 by Velázquez et al. (2004).
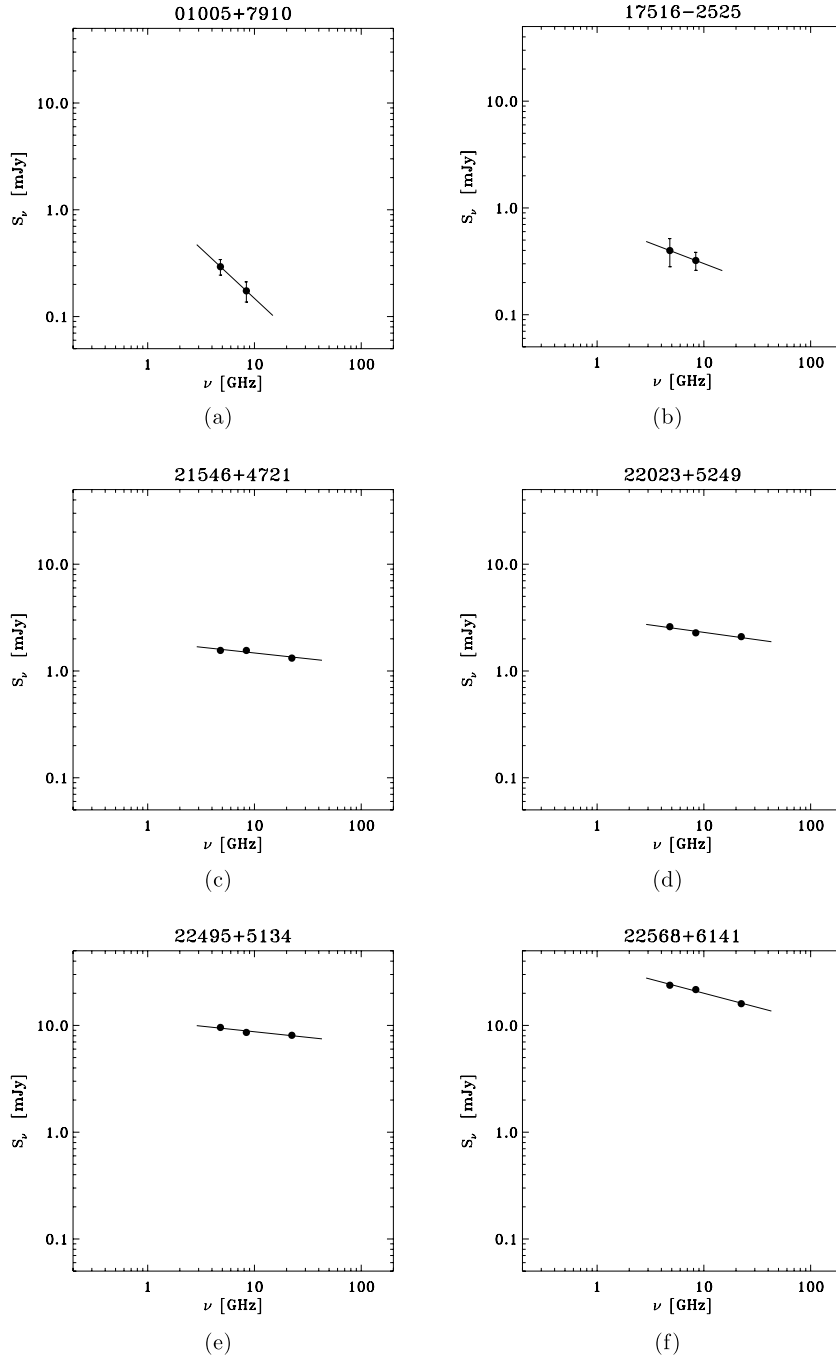
Figure 1. Continuum spectra for targets that had not been observed before at radio wavelengths or that lacked multifrequency observations.

Our 2009 observations indicate that the emission is optically thin, with a spectral index of -0.4 (Table 2). Nevertheless, the observations reported in Cerrigone et al. (2008) at 8.4 and 22.4 GHz indicate optically thick emission between these frequencies with a spectral index around 1. In the cited paper, it was assumed that no variation had occurred in the source between 2001 (epoch of the 8.4 GHz data) and 2003 (epoch of the 22.4 GHz data). Fig. 2 shows that this assumption is not correct and that in 2003 the flux density at 8.4 GHz was smaller than in 2001, if the variability is regular. This does not affect the conclusion that the spectral index was positive in 2003 and likely around 1, considering errors.

If the radio emission is due to the stellar wind, the radius R of the emitting region depends on the frequency as $R(\nu) \sim \nu^{-0.7}$ (Panagia & Felli 1975), in the optically thick regime, as is the case in the 2003 observations. Since any variation in the wind will propagate outwards and the emission at higher frequency arises from inner regions, a light curve at a lower frequency will be delayed compared to one at a higher frequency. Therefore, the value of the spectral index will also vary with time, being positive when the emission is decreasing and negative when it is increasing. The measurement of a positive spectral index in 2003 and a negative one in 2009 strengthens the interpretation of the observed variability as due to

Table 2. Spectral indices from data fitting (with statistical errors), emission measures (lower limit) and beam sizes of the 8.4-GHz data. The list is divided into sources previously detected (upper list) and new detections (lower list).

Target	Spectral index	Emission measure (10^5 cm^{-6} pc)	Beam (arcsec^2)
06556+1623	0.10 ± 0.47	2.6 ± 0.2	3.1×1.3
17381−1616	-0.02 ± 0.22	2.6 ± 0.1	4.7×2.8
17423−1755	-0.40 ± 0.47	0.78 ± 0.07	4.9×2.8
17460−3114	-0.51 ± 0.35	1.30 ± 0.08	6.9×2.6
18062+2410	0.78 ± 0.20	$-^a$	3.0×2.7
18442−1144	-0.09 ± 0.15	38.2 ± 0.1	4.2×2.8
19336−0400	-0.27 ± 0.15	20.4 ± 0.1	3.6×2.7
19590−1249	-0.13 ± 0.17	9.4 ± 0.1	3.0×2.3
20462+3416	-0.67 ± 0.46	2.0 ± 0.2	2.6×1.7
01005+7910	-0.93 ± 0.98	0.8 ± 0.2	2.8×1.7
17516−2525	-0.38 ± 1.29	0.5 ± 0.1	5.7×2.2
21546+4721	-0.11 ± 0.09	7.8 ± 0.2	2.7×1.6
22023+5249	-0.14 ± 0.08	8.6 ± 0.2	2.6×2.1
22495+5134	-0.11 ± 0.06	11.7 ± 0.2	5.3×2.9
22568+6141	-0.26 ± 0.05	$-$	$-$
22568+6141 N	-0.14 ± 0.02	148 ± 4	2.0×0.8
22568+6141 S	-0.20 ± 0.04	123 ± 4	2.0×0.8

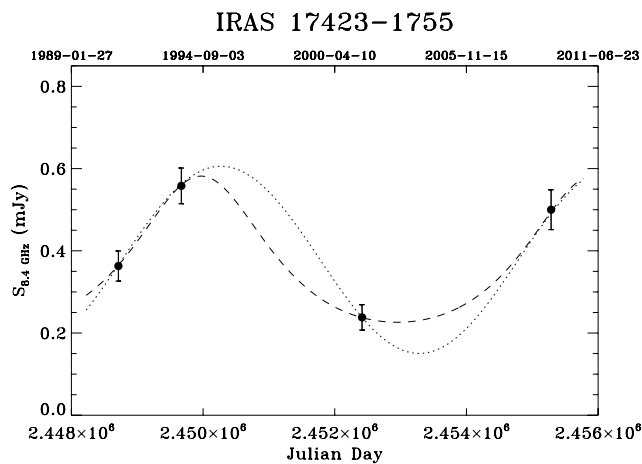^{a}Not optically thin: see modelling in Section 6.

IRAS 17423−1755

Figure 2. VLA observations at 8.4 GHz of IRAS 17423−1755 over 16 yr. The point in 1991 is from the VLA project AK247 (PI: Knapp), while that in 1993 is from AZ63 (PI: Zijlstra).

an unstable stellar wind. As shown in Panagia & Felli (1975), if the radio flux is due to a stellar wind, we can calculate its mass-loss rate as

$$\dot{M} = 0.32 \times 10^{-5} \frac{v_\infty}{10^3 \text{ km s}^{-1}} \left(\frac{F_\nu}{\text{mJy}}\right)^{3/4} \left(\frac{D}{\text{kpc}}\right)^{3/2} \text{ M}_\odot \text{ yr}^{-1}$$

and the size of the emitting region as

$$R(\nu) = 6.23 \times 10^{14} \left(\frac{\nu}{10 \text{ GHz}}\right)^{-0.7} \left(\frac{\dot{M}}{10^{-5} \text{ M}_\odot \text{ yr}^{-1}}\right)^{2/3}$$
$$\cdot \left(\frac{v_\infty}{10^3 \text{ km s}^{-1}}\right)^{-2/3} \text{ cm},$$

where cosmic abundances, full ionization and a 10^4 K temperature of the electron gas have been assumed. If we link the radio flux to the fast wind component, then we can take 100 km s^{-1} as its terminal velocity and calculate from the radio flux density in 2001 (when the spectral index was likely positive) $\dot{M} \sim 1.6 \times 10^{-6} \text{ M}_\odot \text{ yr}^{-1}$

and $R_{8.4\,\text{GHz}} \sim 10^{15}$ cm (~ 0.01 arcsec), assuming a distance of 5.8 kpc.

The mass-loss rate found is quite high for a post-AGB star, where values smaller than 10^{-7} M$_\odot$ yr^{-1} are expected. Nevertheless, large rates (10^{-5}–10^{-4} M$_\odot$ yr^{-1}) have been estimated in the prototypical pre-PN CRL 618, which has undergone at least two distinct episodes of mass-loss in the form of a slow wind, in the last 2500 yr (Sánchez-Contreras et al. 2004). Also, enhanced mass-loss in IRAS 17423−1755 has been found by Huggins et al. (2004) who have estimated that its molecular envelope (~ 0.6 M$_\odot$) was ejected in less than 1500 yr at a mass-loss rate $> 10^{-4}$ M$_\odot$ yr^{-1}. The estimation of the linear size of the emitting region allows us to improve the calculation of the emission measure and convert it into an electron density of 2×10^6 cm^{-3}.

If we assume that, like in CRL 618, the radio flux arises from a slow stellar wind (15 km s^{-1}), its mass-loss rate becomes 2.4×10^{-7} M$_\odot$ yr^{-1}, with $R_{8.4}$ approximately unchanged. The lack of multi-epoch observations covering the whole cm range does not allow for conclusiveness.

5 IRAS 17516−2525

This source was first studied by Van der Veen et al. (1989), who had selected it as a post-AGB candidate because of its *IRAS* colours. Hydroxil maser lines with $\Delta v \sim 40 \text{ km s}^{-1}$ were detected with the Parkes and Nançay radiotelescopes by te Lintel Hekkert et al. (1991) and Szymczak & Gerard (2004), respectively; the latter detected both 1612 and 1667 MHz lines. Nevertheless, Van der Veen et al. (1989) did not detect the OH 1612 MHz line with the VLA in B array at the coordinates of the source, but ~ 7 arcmin north of it. Then it is likely then that the detections performed with the single-dish telescopes are to be associated to this offset maser, although further interferometric observations would be desirable to rule out an intrinsic OH variability. Sánchez-Contreras et al. (2008) performed optical spectroscopy of IRAS 17516−2525 and found that its spectrum is dominated by nebular emission lines. They also suggest the presence of a hot central star, based on the similarity between its spectrum and that of IRAS 19520+2759, which they classify as O9. In their analysis of the optical spectrum, Sánchez-Contreras et al. (2008) find that Hα has a P Cyg profile, indicative of ongoing mass-loss, although Pa lines do not display the same profile. Furthermore, they detect the [Ca II] doublet at 7291.47 and 7323.89 Å, which leads them to conclude that moderate-velocity ($40 < v < 100 \text{ km s}^{-1}$) shocks must propagate in the envelope around this star and destruct dust grains, enhancing the amount of Ca in the gas phase, which would otherwise be depleted on to grains.

We detected IRAS 17516−2525 for the first time in 2005 and find a strong decrease in its flux density over 4 yr (11 per cent per year), the source having almost halved its emission at 8.4 GHz. The spectral index between 4.8 and 8.4 GHz indicates an optically thin spectrum, although the detection at the lower frequency is only marginal. In the context of the observations available in the literature, the radio continuum variability may be due to instabilities of the stellar wind (i.e. shocks) propagating in the CSE. More and more sensitive observations are needed to inspect this target and determine its radio continuum spectrum, to possibly distinguish between an ionized shell and a stellar wind and to look for a variability pattern. Within the uncertainty due to the larger error at the lower frequency, our estimate of a flat radio spectral index strengthens the hypothesis that this is a young PN.

6 IRAS 18062+2410

This source has been monitored at optical wavelengths over a wide period of time and shows photometric variability on both short (hours) and long (years) time-scales. In particular, the equivalent widths of Hα and Hβ increase and its optical continuum decreases (Arkhipova et al. 2007). While the short-time variability has been explained in terms of stellar pulsations and an unstable stellar wind, the long-time-scale variations have been attributed to an increase in the degree of ionization of the envelope, due to a stellar temperature increasing at a rate of about 200 K per year (Arkhipova et al. 2007).

Previous VLA observations of this target performed in 2003 and 2005 are reported in Cerrigone et al. (2008). We have modelled the radio continuum emission, assuming that the central star is surrounded by a shell of ionized gas with density radially decreasing as r^{-2}. We have calculated a 3D distribution of mass in a spherical shell with an outer radius R_{out}, inner radius $R_{in} = \eta R_{out}$ (with $0 < \eta < 1$) and density at the inner radius ρ_{in}. The calculation of the average density in the shell links this parameter to the density at the inner radius: $\langle \rho \rangle \approx \eta^2 (1 - \eta)\rho_{in}$. The electron temperature was set to 10^4 K. Details of the radio model can be found in Umana et al. (2008). We fit the 2003 data with $R_{in} = 0.0354$ arcsec, $R_{out} = 0.06$ arcsec, $\rho_{in} = 5.2 \times 10^5$ cm^{-3} and $d = 6.4$ kpc, which gives us an estimated ionized mass of about 1.48×10^{-4} M$_\odot$.

The nebula has increased its flux density in 2005 and 2009, as shown in Fig. 3. To estimate the expansion velocity of the ionization front, we assume that the CSE expands at a typical velocity of 15 km s^{-1} (therefore, its inner radius will be 0.0364 arcsec in 2005). A fit to the 2005 data enables us to calculate that the velocity of the ionization front is of the order of 100–200 km s^{-1}, the typical range for fast winds in post-AGB stars.

Having the above-mentioned values as first guesses, we now try to fit all of the 2001–2009 data, keeping the CSE expansion velocity set at 15 km s^{-1}. We first set R_{in0}, R_{out0} (the values in 2001), ρ_{in0} (the density at R_{in0}, which does not vary with the epoch) and v_{out} (the velocity of the ionization front within the shell). Then we calculate $R_{in} = R_{in0} + v_{in}\Delta t$ and $R_{out} = R_{out0} + (v_{in} + v_{out})\Delta t$ for the other epochs, Δt being the time between the first observation and the specific epoch; finally, we calculate the density at R_{in} as $\rho_{in} = \rho_{in0}(\frac{R_{in0}}{R_{in}})^2$. A satisfactory fit can be obtained if $v_{out} = 120$ km s^{-1} (kept constant at all epochs) and in 2001 we have $R_{in} =$

0.0380 arcsec, $R_{out} = 0.0522$ arcsec and $\rho_{in} = 5.38 \times 10^5$ cm^{-3}, as shown in Fig. 3.

The models allow us to estimate that the critical frequency has decreased from around 8.2 GHz in 2001 to 7.6 GHz in 2009, pointing to an optical thinning of the envelope, with the opacity at 8.4 GHz ranging between 0.96 in 2001 and 0.84 in 2009. The ionized masses are $1.0 \times 10^{-4}, 1.5 \times 10^{-4}, 2.2 \times 10^{-4}$ and 3.3×10^{-4} M$_\odot$, respectively, in 2001, 2003, 2005 and 2009.

Although a linear increase in the flux density produces a good fit to the data, it cannot rule out the possibility of a cyclic variability with a period much longer than 6 yr.

Fig. 4 shows the variability that we find in this object, which confirms what reported in Cerrigone et al. (2008). We have overplotted the 8.4 GHz flux density calculated from the Hβ fluxes in Arkhipova et al. (2007), which we have estimated from the equivalent widths and absolute values in 1996 and 2006 given in that work. Arkhipova et al. (2007) estimate that the Hβ flux was $(2.7 \pm 0.3) \times 10^{-13}$ erg cm^{-2} s^{-1} in 1995–96 and $(6.2 \pm 0.4) \times 10^{-13}$ erg cm^{-2} s^{-1} in 2006, and list its equivalent width over 10 yr. To convert the equivalent width into flux, we have calculated the average width over all of the 1995–96 observations (one single high point was neglected) and over the 2006 data, then scaled the average values to the respective fluxes given in the paper and finally averaged these two scaling factors together to obtain one mean equivalent width/flux conversion factor. After converting into flux units, each equivalent width, these were converted into radio flux densities at 8.4 GHz following equation (IV-26) in Pottasch (1984):

$$S_\nu = 2.51 \times 10^7 T_e^{0.53} \nu^{-0.1} Y F_{H\beta},$$

where S_ν is the flux density in Jy at the frequency ν, T_e is the electron temperature (set to 10^4 K), ν is in GHz, Y accounts for contributions from He ions and is set to 1.1 and $F_{H\beta}$ is the flux in Hβ in units of erg cm^{-2} s^{-1}.

The mismatch between the two data sets in Fig. 4 is likely due to an optical depth effect. As we have shown in our modelling, the nebula is undergoing optical thinning of its envelope. When the radio flux density is optically thick, its observed value will be smaller than that calculated from the Hβ flux; on the contrary, when it is optically thin, it will be larger than the value calculated from the Hβ flux, because of absorption at optical wavelengths. Fig. 4 seems to be showing the passage from one regime to the other. The Hβ data seem to show a periodicity before 2002. After excluding three
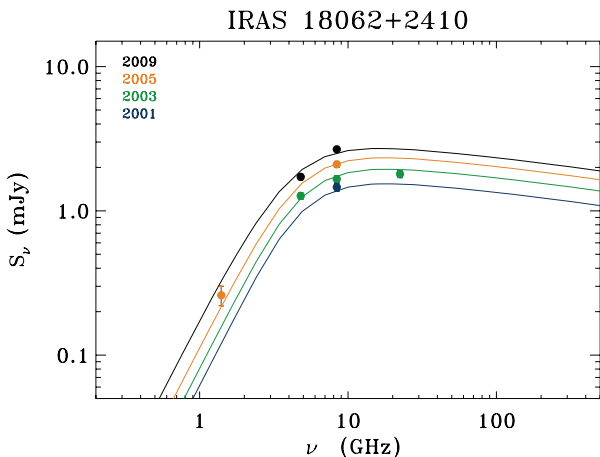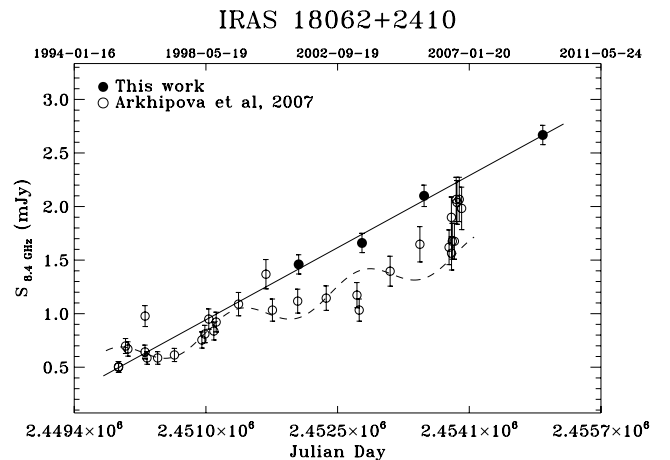

Figure 3. Radio continuum spectra of IRAS 18062+2410 obtained at different epochs. The correspondent model curves are shown in the same colour as the data points.

Figure 4. Radio flux density at 8.4 GHz and Hβ flux (Arkhipova et al. 2007) at several epochs for IRAS 18062+2410. The dashed curve is a fit to the Hβ points before 2002.

clear outsider points, we have calculated a fit to the data before 2002 with a functional form of type $F_{\mathrm{H}\beta} = A_0 \sin(2\pi t/A_1) + A_2 t + A_3$, which includes a periodic term and a linearly increasing one. This fit gives a period of ~4.1 yr and a starting time of ~6.3 yr before the first observation ($A_0 = 0.47, A_1 = 1500, A_2 = 8.7172 \times 10^{-4}, A_3 = -2133.622$).

The number of Lyman photons necessary to sustain the ionized region can be calculated as

$$Q = V n_{\mathrm{e}}^2 \alpha_B,$$

where V is the volume of the ionized region, n_{e} is the average electron density and α_B is the recombination coefficient summed over all the excited states (2.59×10^{-13} cm^3 s^{-1}, at $T_{\mathrm{e}} = 10^4$ K) (Kwok 2000a). Taking advantage of the parameters derived from our modelling, we can estimate that in 2001 $Q = 2.2 \times 10^{46}$ photon s^{-1}, while in 2009 $Q = 1.0 \times 10^{47}$ photon s^{-1}, which by interpolating the values in Panagia (1973) give temperatures of the central star of ~23 400 and ~25 900 K in 2001 and 2009, respectively.

7 IRAS 22568+6141

IRAS 22568+6141 was discovered by García-Lario et al. (1991) who classified it as a possible young PN and estimated a distance of 6 kpc, electron density of about 2×10^4 cm^{-3} and $T_{\mathrm{eff}} \sim 24\,000$ K. For this source, a comparison with previous data is possible only at one frequency. We first detected this nebula with the VLA (C array) in 2005 July at 8.4 GHz and found a flux density of 32.70 ± 0.98 mJy (Umana et al, in preparation). The source was also included in a survey carried out with the Torun 32-m Radio Telescope between 2005 December and 2007 May by Pazderska et al. (2009). They measured 31.4 ± 4.1 mJy at 30 GHz, which is in agreement with our measurement at 8.4 GHz, because we find that the emission is optically thin.

Our observations indicate a decrease in the emission of around 34 per cent between 2005 and 2009. Since the source is known to be extended and we observed it with an interferometer in different array configurations, missing flux could be the reason of the apparent variability. Interferometers in fact filter out emission from structures beyond a size – the largest angular scale (LAS) – that depends on the shortest baseline and on the *uv* coverage. Our low-frequency observations were carried out during reconfiguration time and the minimum baselines turned out to be around 1.3 and 2.1$k\lambda$ at 4.8 and 8.4 GHz, respectively. These correspond respectively to a LAS of around 40 and 23 arcsec, respectively, in snapshot mode. The high-frequency run was performed in D array, with a LAS ~ 33 arcsec. It is therefore unlikely that we are missing any flux from extended structures, since this source is known to have a size of around 8 arcsec from observations in other wavelength ranges (Sahai et al. 2007). We can conclude that the fading of the nebula is real.

Fig. 5 shows the double-peak morphology found in the target, which matches what observed at optical and near-IR wavelengths. The southern peak is not resolved in any of our maps, while the northern one is partly resolved with a size of around 2.0×0.8 arcsec^2 (PA $\sim 50°$). The emission measures are 12.3×10^6 and 14.8×10^6 cm^{-6} pc, for the southern and northern lobe, respectively, where the same size has been used for both blobs.

If we assume a distance to the nebula of 6 kpc, then from the emission measure, we find densities of 2.0×10^4 cm^{-3} (north peak) and 1.8×10^4 cm^{-3} (south peak). The corresponding decay times for electron recombination are $t_{\mathrm{decay}} = \frac{7.6 \times 10^4}{(n_{\mathrm{e}}/\mathrm{cm}^{-3})}$ yr (Kwok 2000a), then about 3.8 and 4.2 yr for the north and south blobs, respectively. For the northern peak, which is partly resolved in our observations, we
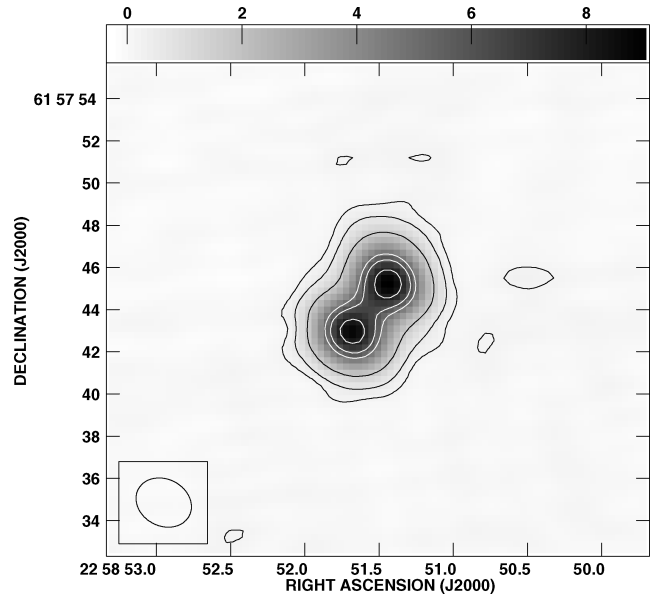

Figure 5. Bipolar morphology observed at 8.4 GHz in IRAS 22568+6141. The contours are $60 \times (-3, 3, 9, 27, 81, 100, 130)$ μJy beam^{-1} and the grey-scale is in mJy beam^{-1}. The convolution beam is shown in the bottom left-hand corner.

also calculate the ultraviolet (UV) luminosity necessary to produce the observed radio flux density as done for IRAS 18062+2410. In this case, we calculate the luminosity as if the star were at the centre of the blob, assuming that the emitting volume is a sphere whose radius equals the geometric mean of the semiaxes from the Gaussian fit. We obtain $Q \sim 4.7 \times 10^{46}$ photon s^{-1}. Because of the geometry of the source, this is to be regarded as a lower limit to the stellar UV luminosity, since the photons ionizing the blob are only a fraction of all those emitted by the central star and many may also be absorbed by circumstellar dust. By interpolation of the values in Panagia (1973) for giant stars (class III), this gives us a lower limit of 24 600 K for the temperature of the central star, slightly larger than what estimated by García-Lario et al. (1991). This lower limit points out a possible rapid increase in the temperature of the central star.

Our observations confirm that this object has started its PN evolutionary phase.

8 CONCLUSIONS

The transition from post-AGB stars to PNe is a crucial point of the evolution of intermediate-mass stars. The development of an ionization front determines major changes in the circumstellar environment and may contribute to the shaping of these intriguing sources. Winds and jets are among the agents responsible for the early shaping of the nebulae during the early post-AGB phase, if not even before.

The ionization of the envelope gives us the possibility to study the action of these agents around the star. Observations at optical wavelengths have pointed out that hot post-AGB stars show photometric variability, which in some instances has a quasi-periodic pattern (Arkhipova et al. 2007).

Within our sample of pre- and young PNe, we have found that four of our targets exhibit radio-continuum variability. In IRAS 18062+2410, the variability consists in a steadily increasing flux density, while in IRAS 17423−1755, it may follow a

periodic pattern. The remaining two variable sources, namely IRAS 17516−2525 and 22568+6141, have both decreased their flux densities by about 10 per cent per year over a 4-yr period. The cause of such a decrease is not clear. They may follow a variability pattern similar to that of IRAS 17423−1755, but in this source the variability occurs in a very compact region around the central star, while in IRAS 22568+6141, it involves two regions likely ∼1.5 arcsec away from the star (1.3×10^{17} cm at 6 kpc).

In near-IR images, the central star in IRAS 22568+6141 appears completely obscured, which implies the presence of a thick circumstellar region of dust and molecular gas. Even at centimetre wavelengths, we do not detect any central emission, although this may be an angular resolution issue. We can speculate that this obscuring region is in fact a circumstellar disc and the two radio blobs are due to the action of a collimated wind on to the circumstellar nebula. In this scenario, if the wind slows down, fewer photons per second will reach the CSE. Because of the high density, the decay time is short and then the radio flux will decrease, as a result of recombinations. In an alternative scenario, we can imagine that the central star is rapidly increasing its temperature, producing more and more photons at shorter wavelengths. In the blackbody approximation, the radiation from the central star peaks at around 1207 Å, if $T_{\rm eff} = 24\,000$ K. Down to about 600 Å for silicates and 800 Å for amorphous carbon, the dust absorption coefficient increases with decreasing wavelength; therefore, the hardening of the radiation from the central star would suffer stronger dust absorption determining a decrease in the ionization degree and in the observed radio flux density, until the radiation manages to destroy the dust grains. A decrease in radio continuum emission over a few years might then indicate a fast increase in stellar temperature. Variability may be present in several other targets in the sample, although the data do not allow for any conclusive statement. Similar results have been obtained for other stars transiting between the late post-AGB and the PN phases, such as CRL 618 (Sánchez-Contreras et al. 2004) and SAO 244567 (Umana et al. 2008).

While a linear increase in time of the flux density points out to the progression of the ionization front in the envelope, quasi-periodic patterns may indicate the presence of jets or instabilities of the stellar wind (i.e. shocks). Several models invoke instabilities and episodic ejections, or quasi-periodic variability. The magneto-hydrodynamic simulations in García-Segura (1997) show that the collimated outflow can be subject to instabilities and form blobs (i.e. the knots observed in pre-PNe) or an episodic jet can be produced by periodic variations in the magnetic field. Such instabilities typically have much longer time-scales than what observed in our targets and cannot be linked directly to our (relatively) short-term variations.

ACKNOWLEDGMENT

REFERENCES

Arkhipova V. P., Ikonnikova N. P., Noskova R. I., Kommisarova G. V., Klochkova V. G., Esipov V. F., 2001, Astron. Lett., 27, 719

Arkhipova V. P., Esipov V. F., Ikonnikova N. P., Komissarova G. V., Noskova R. I., 2007, Astron. Lett., 33, 604

Blackman E. G., Frank A., Markiel J. A., Thomas J. H., Van Horn H. M., 2001, Nat, 409, 485

Bobrowsky M., Sahu K. C., Parthasarathy M., García-Lario P., 1999, Nat, 392, 469

Cerrigone L., Umana G., Trigilio C., Leto P., Buemi C. S., Hora J. L., 2008, MNRAS, 390, 363

García-Segura G., 1997, ApJ, 489, L189

García-Lario P., Manchado A., Riera A., Mampaso A., Pottasch S. R., 1991, A&A, 249, 223

Hrivnak B. J., Lu W., Maupin R. E., Spitzbart B. D., 2010, ApJ, 709, 1042

Huggins P. J., Muthu C., Bachiller R., Forveille T., Cox P., 2004, A&A, 414, 581

Kahn F. D., West K. A., 1985, MNRAS, 212, 837

Kwok S., 2000a, The Origin and Evolution of Planetary Nebulae. Cambridge Univ. Press, Cambridge

Kwok S., 2000b, in Kastner J. H., Soker N., Rappaport S., eds, ASP Conf. Ser. Vol. 199, Asymmetrical Planetary Nebulae II: from Origins to Microstructures. Astron. Soc. Pac., San Francisco, p. 9

Kwok S., Purton C. R., Fitzgerald P. M., 1978, ApJ, 219, L125

Lee C.-F., Sahai R., 2003, ApJ, 586, 319

Panagia N., 1973, AJ, 78, 929

Panagia A., Felli M., 1975, A&A, 39, 1

Pazderska B. M. et al., 2009, A&A, 498, 463

Pottasch S. R., 1984, Planetary Nebulae – A Study of Late Stages of Stellar Evolution. D. Reidel Publishing Co. (Astrophysics and Space Science Library), Dordrecht

Riera A., García-Lario P., Manchado A., Bobrowsky M., Estalella R., 2003, A&A, 401, 1039

Sahai R., Trauger J. T., 1998, AJ, 116, 1357

Sahai R., Morris M., Sánchez Contreras C., Claussen M., 2007, AJ, 134, 2200

Sánchez Contreras C., Sahai R., 2001, ApJ, 553, L173

Sánchez Contreras C., Bujarrabal V., Castro-Carrizo A., Alcolea J., Sargent A., 2004, ApJ, 617, 1142

Sánchez Contreras C., Sahai R., Gil de Paz A., Goodrich R., 2008, ApJ, 179, 166

Soker N., 2006, ApJ, 645, L57

Suárez O., García-Lario P., Manchado A., Manteiga M., Ulla A., Pottasch S. R., 2006, A&A, 458, 173

Szymczak M., Gérard E., 2004, A&A, 423, 209

te Lintel Hekkert P., Caswell J. L., Habing H. J., Haynes R. F., Norris R. P., 1991, A&AS, 90, 327

Terzian Y., Dickey J., 1973, AJ, 78, 875

Umana G., Cerrigone L., Trigilio C., Zappalà R. A., 2004, A&A, 428, 121

Umana G., Trigilio C., Cerrigone L., Buemi C. S., Leto P., 2008, MNRAS, 386, 1404

van der Veen W. E. C. J., Habing H. J., van Langevelde H. J., Geballe T. R., 1989, A&A, 216, L1

Velázquez P. F., Riera A., Raga A. C., 2004, A&A, 419, 991

This paper has been typeset from a TEX/LATEX file prepared by the author.